+10 mV (see Supplementary Information). The size of the leak was adjusted to produce the same steady-state depolarization in the model as occurred in light-adapted photoreceptors (Fig. 1b). The log-normal shape of the light conductance pulses (Fig. 5) was fitted to experimentally derived light impulse responses[12], and the size of pulses was adjusted so that the largest conductance pulse produced a saturated voltage response with an amplitude similar to that seen in experiments.

To ensure that the Hodgkin–Huxley-type model could be driven with the same dynamic white noise that was used in experiments[30], we tested it by removing the active conductances, thereby reducing it to an analytically solvable RC circuit. A comparison of the model output with the exact solution of the RC circuit in the frequency domain showed that the numerical methods used in the model did not introduce errors. Identical stimuli were used in both modelling and *in vivo* recordings to allow their responses to be compared directly.

Received 1 November; accepted 2 December 2002; doi:10.1038/nature01384.

1. Hille, B. *Ionic Channels of Excitable Membranes* 3rd edn (Sinauer Associates, Sunderland, Massachusetts, 2001).
2. Rudy, B. Diversity and ubiquity of K^+ channels. *Neuroscience* **25,** 729–749 (1988).
3. Coetzee, W. A. *et al.* Molecular diversity of K^+ channels. *Ann. NY Acad. Sci.* **868,** 233–285 (1999).
4. Sheng, M., Liao, Y. J., Jan, Y. N. & Jan, L. Y. Presynaptic A-current based on heteromultimeric K^+ channels detected *in vivo*. *Nature* **365,** 72–75 (1993).
5. Wang, H., Kunkel, D. D., Martin, T. M., Schwartzkroin, P. A. & Tempel, B. L. Heteromultimeric K^+ channels in terminal and juxtaparanodal regions of neurons. *Nature* **365,** 75–79 (1993).
6. Salkoff, L. & Wyman, R. Genetic modification of potassium channels in *Drosophila Shaker* mutants. *Nature* **293,** 228–230 (1981).
7. Kaplan, W. D. & Trout, W. E. The behaviour of four neurological mutants of *Drosophila*. *Genetics* **61,** 399–409 (1961).
8. Hardie, R. C., Voss, D., Pongs, O. & Laughlin, S. B. Novel potassium channels encoded by the *Shaker* gene in *Drosophila* photoreceptors. *Neuron* **6,** 477–486 (1991).
9. Hardie, R. C. Voltage-sensitive potassium channels in *Drosophila* photoreceptors. *J. Neurosci.* **11,** 3079–3095 (1991).
10. Hardie, R. C. & Raghu, P. Visual transduction in *Drosophila*. *Nature* **413,** 186–193 (2001).
11. Weckström, M. & Laughlin, S. B. Visual ecology and voltage-gated ion channels in insect photoreceptors. *Trends Neurosci.* **18,** 17–21 (1995).
12. Juusola, M. & Hardie, R. C. Light adaptation in *Drosophila* photoreceptors: I. Response dynamics and signaling efficiency at 25 °C. *J. Gen. Physiol.* **117,** 3–25 (2001).
13. Laurent, G. Voltage-dependent nonlinearities in the membrane of locust nonspiking local interneurons, and their significance for synaptic integration. *J. Neurosci.* **10,** 2268–2280 (1990).
14. Hoffman, D. A., Magee, J. C., Colbert, C. M. & Johnston, D. K^+ channel regulation of signal propagation in dendrites of hippocampal pyramidal neurons. *Nature* **387,** 869–875 (1998).
15. Magee, J., Hoffman, D., Colbert, C. & Johnston, D. Electrical and calcium signaling in dendrites of hippocampal pyramidal neurons. *Annu. Rev. Physiol.* **60,** 327–346 (1998).
16. Connor, J. A. & Stevens, C. F. Voltage clamp studies of a transient outward membrane current in gastropod neural soma. *J. Physiol. (Lond.)* **213,** 21–30 (1971).
17. Debanne, D., Guérineau, N. C., Gähwiler, B. H. & Thompson, S. M. Action-potential propagation gated by an axonal I_A-like K^+ conductance in hippocampus. *Nature* **389,** 286–289 (1997).
18. de Ruyter van Steveninck, R. R. & Laughlin, S. B. The rate of information transfer in graded-potential neurons and chemical synapses. *Nature* **379,** 642–645 (1996).
19. Laughlin, S. B. A simple coding procedure enhances a neurone's information capacity. *Z. Naturforsch.* **36,** 910–912 (1981).
20. Kouvalainen, E., Weckström, M. & Juusola, M. Determining photoreceptor signal-to-noise ratio in the time and frequency domains with a pseudorandom stimulus. *Vis. Neurosci.* **95,** 1221–1225 (1994).
21. Shannon, C. E. Communication in the presence of noise. *Proc. Inst. Radio Eng.* **37,** 10–21 (1948).
22. Bendat, J. S. & Piersol, A. G. *Random Data: Analysis and Measurement Procedures* (Wiley & Sons, New York, 1971).
23. Hodgkin, A. L. & Huxley, A. F. A quantitative description of membrane current and its application to conduction and excitation in nerve. *J. Physiol. (Lond.)* **117,** 500–544 (1952).
24. Johnston, D. & Wu, S. M.-S. *Foundations of Cellular Neurophysiology* (MIT Press, Cambridge, Massachusetts, 1995).
25. Desai, N. S., Cudmore, R. H., Nelson, S. B. & Turrigiano, G. G. Critical periods for experience-dependent synaptic scaling in visual cortex. *Nature Neurosci.* **5,** 783–789 (2002).
26. Stemmler, M. & Koch, C. How voltage-dependent conductances can adapt to maximize the information encoded by neuronal firing rate. *Nature Neurosci.* **2,** 521–527 (1999).
27. Brickley, S. G., Revilla, V., Cull-Candy, S. G., Wisden, W. & Farrant, M. Adaptive regulation of neuronal excitability by a voltage-independent potassium conductance. *Nature* **409,** 88–92 (2001).
28. Henderson, S. R., Reuss, H. & Hardie, R. C. Single photon responses in *Drosophila* photoreceptors and their regulation by Ca^{2+}. *J. Physiol. (Lond.)* **524,** 179–194 (2000).
29. Hevers, W. & Hardie, R. C. Serotonin modulates the voltage dependence of delayed rectifier and *Shaker* potassium channels in *Drosophila* photoreceptors. *Neuron* **14,** 845–856 (1995).
30. Shampine, L. F. & Reichelt, M. W. The MATLAB ODE suite. *SIAM J. Sci. Comput.* **18,** 1–22 (1997).

Supplementary Information accompanies the paper on *Nature*'s website (http://www.nature.com/nature).

Acknowledgements We thank G. Garcia de Polavieja and H. Robinson for comments on an earlier version of this manuscript. The work was supported by the Royal Society (M.J. and R.C.H.) and the Wellcome Trust (M.J., J.N. and R.C.H.).

Competing interests statement The authors declare that they have no competing financial interests.

Correspondence and requests for materials should be addressed to M.J. (e-mail: mj216@cus.cam.ac.uk).

Ankyrin-B mutation causes type 4 long-QT cardiac arrhythmia and sudden cardiac death

Peter J. Mohler*†, Jean-Jacques Schott†‡, Anthony O. Gramolini*, Keith W. Dilly§, Silvia Guatimosim§, William H. duBell||, Long-Sheng Song§, Karine Haurogné‡, Florence Kyndt‡, Mervat E. Ali*, Terry B. Rogers||, W. J. Lederer§, Denis Escande‡, Herve Le Marec‡¶ & Vann Bennett*#

* *Howard Hughes Medical Institute and Departments of Cell Biology, Biochemistry, and Neuroscience, Duke University Medical Center, Durham, North Carolina 27710, USA*
‡ *Laboratoire de Physiopathologie et de Pharmacologie Cellulaires et Moléculaires, INSERM U533, Hôtel-Dieu; and* ¶ *Département de Cardiologie, Hôspital G&R Laennec, Nantes, France*
§ *Medical Biotechnology Center and Department of Physiology, University of Maryland Biotechnology Institute; and* || *Department of Biochemistry & Molecular Biology, University of Maryland School of Medicine, Baltimore, Maryland 21021, USA*
† *These authors contributed equally to this work*

Mutations in ion channels involved in the generation and termination of action potentials constitute a family of molecular defects that underlie fatal cardiac arrhythmias in inherited long-QT syndrome[1]. We report here that a loss-of-function (E1425G) mutation in ankyrin-B (also known as ankyrin 2), a member of a family of versatile membrane adapters[2], causes dominantly inherited type 4 long-QT cardiac arrhythmia in humans. Mice heterozygous for a null mutation in ankyrin-B are haploinsufficient and display arrhythmia similar to humans. Mutation of ankyrin-B results in disruption in the cellular organization of the sodium pump, the sodium/calcium exchanger, and inositol-1,4,5-trisphosphate receptors (all ankyrin-B-binding proteins), which reduces the targeting of these proteins to the transverse tubules as well as reducing overall protein level. Ankyrin-B mutation also leads to altered Ca^{2+} signalling in adult cardiomyocytes that results in extrasystoles, and provides a rationale for the arrhythmia. Thus, we identify a new mechanism for cardiac arrhythmia due to abnormal coordination of multiple functionally related ion channels and transporters.

We previously characterized a large French kindred (Fig. 1a) where long-QT syndrome associated with sinus node dysfunction and episodes of atrial fibrillation segregated as an autosomal-dominant trait mapping to an 18-cM interval on chromosome 4q25-27 (ref. 3). Among the 25 affected patients (21 adults and 4 children) included in the study, average rate-corrected QT interval (QTc) was 490 ± 30 ms (for adults) and 465 ± 38 ms (for children) compared with 380 ± 30 ms and 403 ± 36 ms in unaffected individuals. T-wave morphologies characterized by sinusoidal features differed from those observed in the long-QT type 1–3 syndrome (LQT1–3). Sinus node bradycardia or junctional escape rhythm was diagnosed in all patients with LQT4 (ref. 3; see also Supplementary Fig. 1), although 24-h electrocardiogram (ECG) recordings revealed that sinus node dysfunction alternated with normal sinus rhythm. Nine patients were equipped with a rate-responsive atrial pacemaker because of marked bradycardia and the need of beta-blocking therapy. Finally, episodes of atrial fibrillation were diagnosed in 12 adult patients but were absent during childhood. Since the initial description of the family, eight additional individuals have been born. Four were demonstrated to carry the LQT4 haplotype. Sinus node abnormalities were diagnosed *in utero* in all affected members from generation IV.

Present address: Box 3892, Duke University Medical Center, Durham, North Carolina 27710, USA.

 © 2003 Nature Publishing Group

Sequencing of the gene encoding ankyrin-B (*ANKB*; also known as *ANK2*) identified an A to G transition mutation at position 4274 in exon 36, resulting in the substitution of glycine for a glutamic acid at amino acid residue 1425 (E1425G) near the regulatory domain of 220-kDa ankyrin-B (Fig. 1b). No nucleotide alterations were identified in two other positional candidate genes encoding CAMKII-δ or TRP3. Forty-five family members (24 carriers, including one individual who suffered sudden death, and 21 non-carriers) were evaluated for the E1425G mutation. The E1425G mutation segregated with LQT in 22 out of 24 individuals (III-5 and IV-1 were non-penetrant, with QTc = 420 ms), and with sinus node dysfunction in 23 out of 24 individuals (III-12 was non-penetrant with a heart rate of 60 beats per min (b.p.m.); Supplementary Fig. 4). The E1425G mutation was not found in more than 400 control alleles.

We evaluated the functional activity of the E1425G mutant on the basis of the ability to rescue abnormal Ca^{2+} dynamics of $AnkB^{+/-}$ neonatal cardiomyocytes obtained from mice heterozygous for a null mutation in the gene encoding ankyrin-B[4,5] (neonatal cardiomyocytes were used because adult cardiomyocytes are not readily transfected). Ankyrin-B expression in $AnkB^{+/-}$ cells is reduced and localized to a striated pattern only in certain regions of these cells (Supplementary Fig. 2). $AnkB^{+/-}$ cardiomyocytes have a decreased spontaneous contraction rate (144 ± 10 to 78 ± 8 b.p.m.; $P < 0.05$) associated with prolonged intracellular Ca^{2+} concentration ($[Ca^{2+}]_i$) transients at a lower frequency (Fig. 1c; from 2.7 to about 1.3 Hz; $P < 0.05$). These defects in $AnkB^{+/-}$ cardiomyocytes can be rescued by transfection with complementary DNA encoding green fluorescent protein (GFP)-tagged 220-kDa ankyrin-B (Fig. 1c; Ca^{2+} waves approximately 2.2 Hz, rhythm restored to 134 ± 11 b.p.m.). In contrast, $AnkB^{+/-}$ cardiomyocytes transfected with ankyrin-B containing the human E1425G mutation still displayed abnormal Ca^{2+} oscillations (Fig. 1c; approximately 1.3 Hz; with instances of prolonged elevations in cytosolic Ca^{2+}; $P < 0.05$) and a decreased beat frequency (71 ± 12 b.p.m.; $P < 0.05$), even though the mutant GFP–ankyrin-B itself targeted normally (Supplementary Fig. 2). Therefore, two normal copies of the ankyrin-B gene are required for normal Ca^{2+} signalling, and the E1425G mutation leads to loss-of-function. Ankyrin-B is, to our knowledge, the first identified protein to be implicated in a congenital long-QT syndrome that is not an ion channel or channel subunit[1,6].

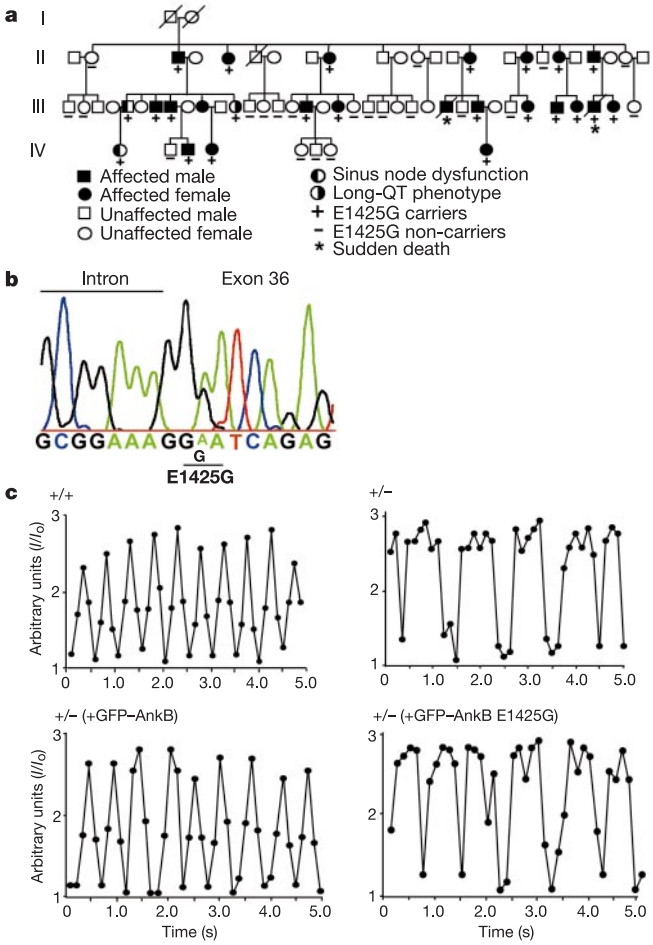

Figure 1 Loss-of-function mutation in ankyrin-B in type 4 long-QT syndrome. **a**, Pedigree of type 4 long-QT family. Filled symbols indicate long-QT and sinus node dysfunction phenotypes. **b**, An A to G mutation at position 4274 causes a E1425G missense mutation. **c**, Ca^{2+} levels as a function of time (fold increase over basal levels (I/I_0)). Graphs represent untransfected (+/+) (top left) and $AnkB^{+/-}$ (+/−) neonatal cardiomyocytes (top right), and GFP–ankyrin-B (bottom left) and GFP–ankyrin-B E1425G (bottom right) transfected $AnkB^{+/-}$ cardiomyocytes. After Ca^{2+} imaging, cardiomyocytes were monitored for GFP–ankyrin-B to ensure transfection.

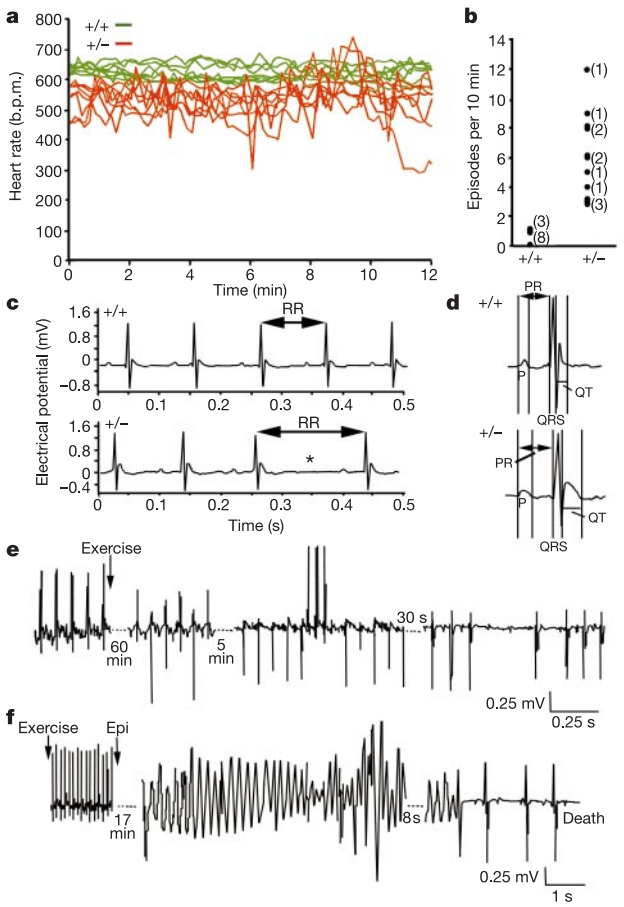

Figure 2 Sinus bradycardia, heart rate variability and sudden cardiac death in $AnkB^{+/-}$ mice. **a**, Heart rates ($n = 7$ for wild-type and $AnkB^{+/-}$ mice) showing bradycardia and variability in $AnkB^{+/-}$ mice. **b**, Episodes of variable heart rate (greater than ±10% mean heart rate per animal) over 10 min ($n = 11$ for wild-type and $AnkB^{+/-}$ mice). **c**, ECG of sinus slowing of a $AnkB^{+/-}$ mouse. **d**, Sample ECGs of $AnkB^{+/-}$ and wild-type mice. **e**, ECG traces of $AnkB^{+/-}$ mice at rest and after exercise. **f**, ECGs after exercise and administration of epinephrine (Epi). Polymorphic ventricular arrhythmias occurred within about 17 min of epinephrine administration, followed by marked bradycardia and death 2 min after the arrhythmia. No wild-type mice exhibited changes in ECG patterns or died after these treatments.

© 2003 Nature Publishing Group

Analysis of ECGs and heart rates of unrestrained animals using implanted radiotransmitter electrodes revealed significant similarities in cardiac phenotype between humans with LQT4 and $AnkB^{+/-}$ mice (Fig. 2). $AnkB^{+/-}$ mice have bradycardia with a conscious resting heart rate of 515 ± 49 b.p.m., compared with 641 ± 31 b.p.m. for wild-type mice ($n = 12$ for wild-type and 14 for $AnkB^{+/-}$ mice; $P < 0.05$). Bradycardia was observed in all $AnkB^{+/-}$ mice, with these mice displaying a heart rate of less than 600 b.p.m. for 87 ± 3.4% of a 30-min interval, whereas wild-type mice spend 4.3 ± 1.7% of the same interval at less than 600 b.p.m. ($n = 10$ for both genotypes; $P < 0.05$). $AnkB^{+/-}$ mice also exhibit a high degree of heart-rate variability (Fig. 2a, b) associated with multiple episodes of abrupt sinus slowing. Figure 2c shows an ECG trace of one episode for a $AnkB^{+/-}$ mouse. The prolonged RR intervals (sinus slowing; asterisk in Fig. 2c) occur on a background of reduced heart rate (Fig. 2a) compared with wild-type mice. Furthermore, $AnkB^{+/-}$ mice exhibit episodes of intermittent isorhythmic atrioventricular dissociation similar to rhythm disturbances present in human LQT4 patients (Supplementary Fig. 3). ECG abnormalities in $AnkB^{+/-}$ mice are not due to electrolyte or obvious structural defects in the heart, as no significant differences between wild-type and $AnkB^{+/-}$ mice were evident in serum K^+, Na^+, Mg^{2+} or Ca^{2+}, and no histopathological defects were detected in heart sections from $AnkB^{+/-}$ mice.

The QTc is significantly prolonged from 25 ± 1.0 to 30 ± 1.1 ms in $AnkB^{+/-}$ mice ($n = 9$ and 11 for wild-type and $AnkB^{+/-}$ mice; $P < 0.05$). The difference in apparent QT length in a mouse ECG could be due to delayed conduction and/or delayed repolarization[7]. ECGs of $AnkB^{+/-}$ mice, in contrast to humans with LQT4, reveal general slowing of conduction with PR intervals increased from 35.9 ± 1.0 to 39.6 ± 0.7 ms, QRS intervals increased from 8.3 ± 0.1 to 11.2 ± 0.2 ms, and P-wave duration increased from 8.2 ± 0.7 to 13.4 ± 0.5 ms ($n = 9$ and 11 for wild-type and $AnkB^{+/-}$ mice; all differences statistically significant, $P < 0.05$). Given that action potentials of adult $AnkB^{+/-}$ cardiomyocytes are not substantially prolonged, the increase in QT interval observed in $AnkB^{+/-}$ mice is probably due to delayed conduction.

Sudden cardiac death in humans with the E1425G mutation occurred after physical exertion and emotional stress (Fig. 1)[3]. We attempted to mimic these circumstances in mice with exercise followed by injection with epinephrine (see Methods). The mice responded in a dramatic manner. Two out of 14 $AnkB^{+/-}$ mice became unresponsive for 3–10 s immediately after exercise alone. Over half of $AnkB^{+/-}$ mice (8 out of 14) died after exercise combined with epinephrine. No wild-type mouse ever became unresponsive or died during these experiments (0 out of 6).

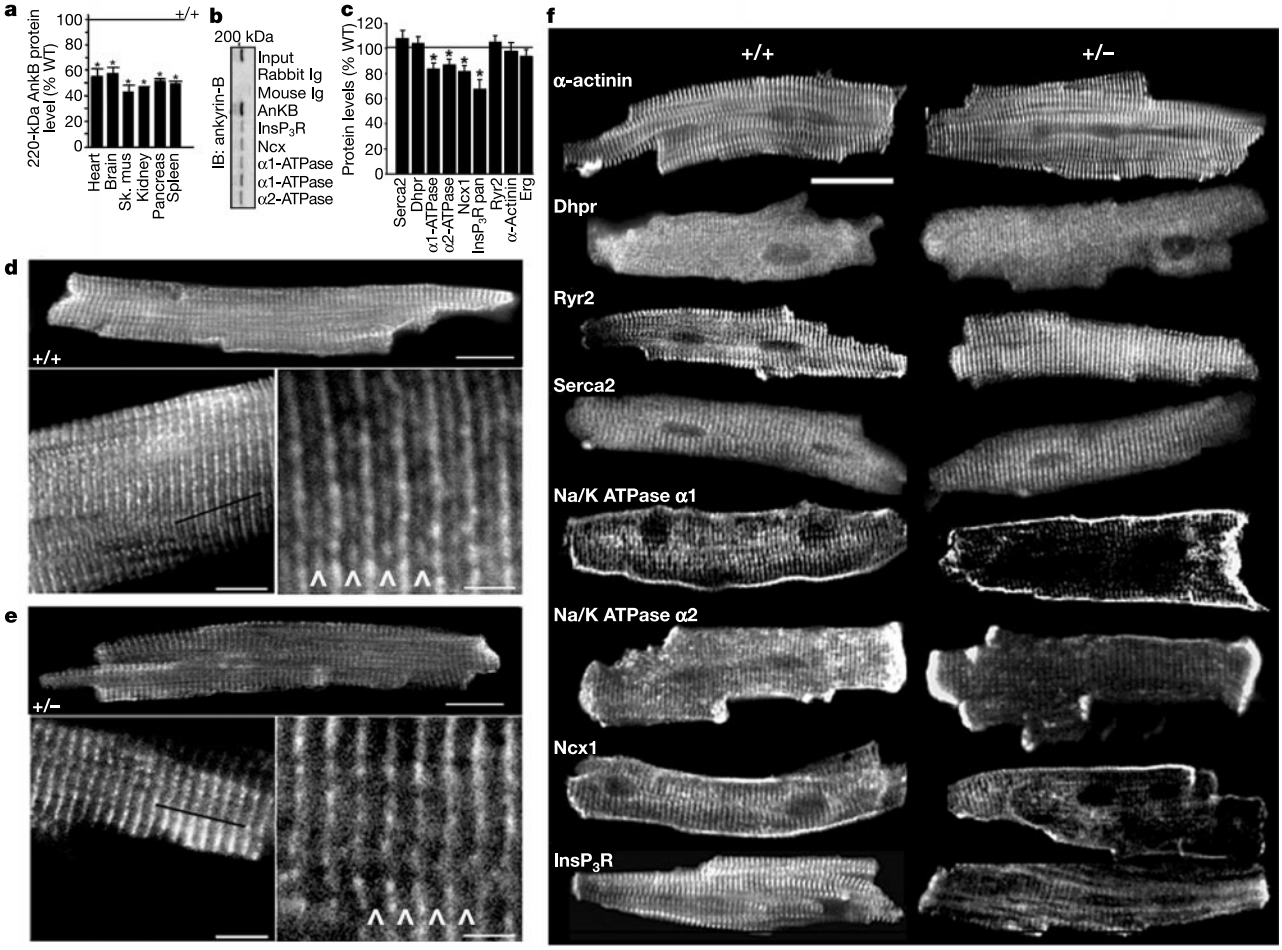

Figure 3 Coordinate reduction of ankyrin-B and ankyrin-B-associated proteins at Z-line/T-tubules of adult $AnkB^{+/-}$ cardiomyocytes. **a**, Quantification of ankyrin-B protein expression in adult tissues ($n = 4$). **b**, Adult cardiomyocyte immunoprecipitations were analysed for 220-kDa ankyrin-B (input = 10% input). **c**, Quantitative immunoblots of protein levels in adult cardiomyocytes ($n = 5$). **d**, **e**, Ankyrin-B immunofluorescence in isolated wild-type and $AnkB^{+/-}$ adult cardiomyocytes (arrowheads indicate Z-lines/T-tubules; scale bars are 20 μm (top), 10 μm (bottom left) and 5 μm (bottom right)). **f**, $AnkB^{+/-}$ cardiomyocytes display qualitative loss of Ncx1, Na/K ATPase α_1 and α_2, and $InsP_3R$ labelling over Z-line/T-tubules. Scale bar, 40 μm. Loss of ankyrin-B-associated protein staining at the Z-line/T-tubule was apparent throughout the entire depth of the cell.

© 2003 Nature Publishing Group

Exercised $AnkB^{+/-}$ mice displayed instances of reversed polarity of the QRS complex (two mice), and second-degree atrio-ventricular block (P-wave with no QRS complex, 11 mice; Fig. 2e). Prolonged polymorphic ventricular arrhythmia immediately preceding death was recorded in two mice treated with exercise plus epinephrine (Fig. 2f). The additional six mice that died from exercise and epinephrine displayed multiple short episodes (1–2 s) of polymorphic ventricular arrhythmia within 0–2 min before death. No arrhythmic episodes were observed in ECGs of wild-type mice after exercise or exercise plus epinephrine.

Reduction in the level of 220-kDa ankyrin-B by about 50% in immunoblots of adult cardiac tissue in $AnkB^{+/-}$ mice (Fig. 3a) is accompanied by selective loss of ankyrin-B staining at the Z-line/transverse (T)-tubule region of $AnkB^{+/-}$ cardiomyocytes (localization at the Z-line/T-tubule based on confocal Z-sections using dihydropyridine receptor (Dhpr) as a T-tubule marker; Fig. 3d). Ankyrin-B staining is retained at the M-line (predominant staining) and intercalated discs (Fig. 3e). Ankyrin-B is also aligned with Z-lines in skeletal muscle, but, in contrast to cardiomyocytes, ankyrin-B in skeletal muscle is restricted to costameres at the sarcolemma[4].

The coordinate loss of ankyrin-binding proteins $Na_V1.6$, beta IV spectrin and neurofascin at axon initial segments lacking ankyrin-G[8] suggested that reduced levels of ankyrin-B at Z-lines/T-tubules in heart could also result in the deficiency of proteins associated with ankyrin-B at T-tubules. Na/K ATPase, Na/Ca exchanger (Ncx) and inositol-1,4,5-trisphosphate receptors ($InsP_3R$) are candidate ankyrin-binding proteins, on the basis of biochemical data[9], that are localized at T-tubules[10]. Ankyrin-B co-immunoprecipitates with Ncx1, the α_1 and α_2 subunits of ATPase, and $InsP_3R$ from extracts of heart tissue (Fig. 3b), but not with other cardiomyocyte proteins (including Dhpr, Serca2 and calsequestrin; data not shown). Immunoblots revealed that levels of $InsP_3R$ (pan $InsP_3R$), α_1 and α_2 Na/K ATPase, and Ncx in isolated adult cardiomyocytes were reduced by 15–33% in $AnkB^{+/-}$ cardiomyocytes (Fig. 3c). Measurements of the binding of $[^3H]InsP_3$ (ligand for $InsP_3R$) and $[^3H]$ouabain (ligand for Na/K ATPase) to adult cardiac microsomes also demonstrated a 33% and 16% reduction, respectively, in capacity in hearts of $AnkB^{+/-}$ mice, whereas affinities for these ligands were unchanged. In contrast, quantitative western blot analysis revealed that protein levels of endoplasmic and sarcoplasmic reticulum components (Serca2, calreticulin, calsequestrin), K^+ channels or associated subunits (Kcnq1/K_VLqt1, Erg1, MinK/IsK, Kir2.1/Irk1, Kir2.3/Irk3), ryanodine receptor 2, plasma membrane Ca^{2+} channels (Dhpr, Pmca2), and structural proteins (α-actinin, dystrophin) were unaffected (Fig. 3c; see also Supplementary Fig. 6). Northern blots revealed no difference in the levels of mRNA encoding $InsP_3R$ (type 1 and pan), Na/K ATPase α_1 and α_2, and Ncx1.

The modest overall reduction in levels of Ncx, Na/K ATPase and $InsP_3R$ has a substantial impact on the levels of these proteins localized at T-tubule sites, which can be detected easily by immunofluorescence (Fig. 3f). Ncx, as well as α_1 and α_2 Na/K ATPase are preferentially reduced in $AnkB^{+/-}$ cardiomyocytes at T-tubule sites, whereas little change can be detected at the sarcolemma or intercalated discs. Furthermore, $InsP_3R$ in $AnkB^{+/-}$ cardiomyocytes is reduced at T-tubule sites and is disorganized in some regions, whereas label at intercalated discs is relatively normal. Markers for T-tubules (Dhpr), the sarcoplasmic reticulum (Serca2), and Z-line components (α-actinin)[10] are unaltered in $AnkB^{+/-}$ cardiomyocytes (Fig. 3f). Proteins that are also unaffected, as monitored by confocal analysis, include dystrophin, connexin 43, $Na_V1.5$, $Na_V1.6$, Erg1, Pmca2, Kcnq1/K_VLqt1, calsequestrin and calreticulin (not shown). Ankyrin-B-dependent expression of $InsP_3R$, Ncx or Na/K ATPase may be a specialized feature of cardiac muscle, as there is no difference in expression or localization of these proteins in skeletal and vascular smooth muscle.

Reduction of Na/K ATPase, Ncx and $InsP_3R$ in neonatal $AnkB^{+/-}$ cardiomyocytes can be rescued by transfection with GFP-tagged 220-kDa ankyrin-B, but not by 220-kDa ankyrin-B containing the E1425G mutation (Supplementary Fig. 2). This indicates that 220-kDa ankyrin-B is necessary and sufficient for normal expression of Ncx, Na/K ATPase and $InsP_3R$ in neonatal cardiomyocytes, and that the same E1425G mutation causing clinical arrhythmia in humans abolishes this activity. These findings establish that ankyrin-B participates in expression of multiple ion-channel/transporter proteins. The current list of ankyrin-B-dependent proteins may not be complete, as the full extent of ankyrin-B-binding partners is not yet known.

Examination of the electrical behaviour and Ca^{2+} dynamics of isolated heart cells from adult $AnkB^{+/-}$ mice with ECG defects revealed a significant increase in the peak $[Ca^{2+}]_i$ level at all potentials (Fig. 4). No significant differences in resting levels of $[Ca^{2+}]_i$ (about 160 nM) were observed using indo-1. An increased $[Ca^{2+}]_i$ transient under these conditions implies that the amount of Ca^{2+} in the sarcoplasmic reticulum is elevated, although these values were not experimentally determined. No significant changes were evident in the magnitude or voltage dependence of the L-type Ca^{2+} channel current between -40 mV and $+60$ mV (I_{Ca}; Fig. 4a). Although heart weights were similar between wild-type and $AnkB^{+/-}$ mice (indicating that no overt hypertrophy accompanied elevated $[Ca^{2+}]_i$), cardiomyocytes of $AnkB^{+/-}$ mice

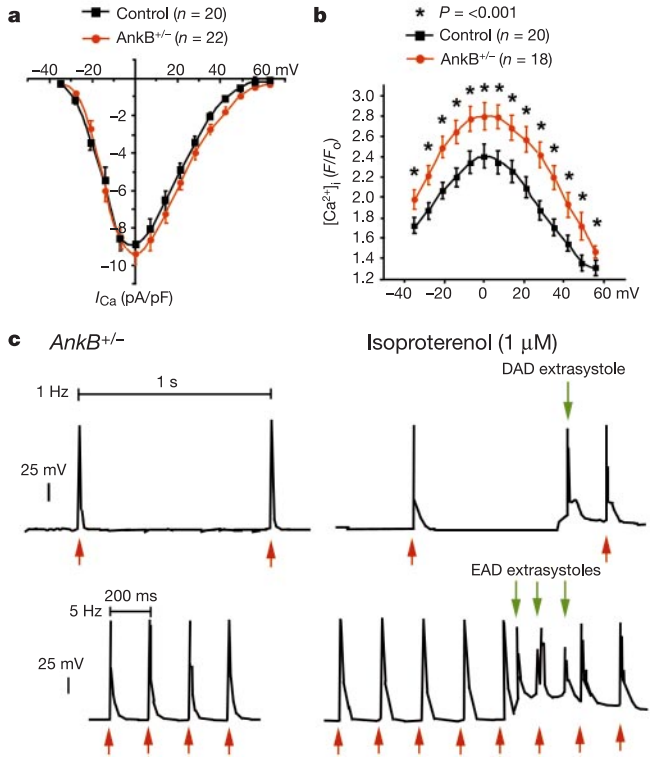

Figure 4 Ca^{2+} signalling in adult $AnkB^{+/-}$ ventricular cardiomyocytes. **a**, I_{Ca} density (0 mV): $AnkB^{+/-}$, 9.37 ± 0.61 pA/pF; control, −8.87 ± 0.60 pA/pF, not significant. **b**, Peak of $[Ca^{2+}]_i$ transient plotted as F/F_0, where F is fluorescence intensity, and F_0 is resting fluorescence intensity. F/F_0 for $AnkB^{+/-}$ is significantly greater than control at all membrane potentials. At 0 mV, F/F_0 for $AnkB^{+/-}$ = 2.80 ± 0.13 (n = 18); control = 2.41 ± 0.12 (n = 20), representing a 16.2% increase. **c**, Steady-state action potentials recorded after 10–20 stimuli from $AnkB^{+/-}$ cardiomyocytes at 1 and 5 Hz in control solutions and in isoproterenol. Red arrows indicate stimuli timing. DADs and EADs were observed in 36% of $AnkB^{+/-}$ cardiomyocytes, but they were not observed in control cardiomyocytes.

© 2003 Nature Publishing Group

did exhibit an approximately 23% increase in capacitance, suggesting increased surface area and a small increase in cell volume.

Cardiac action potentials measured in the presence and absence of isoproterenol revealed stress-induced abnormalities in *AnkB*$^{+/-}$ heart cells (Fig. 4c). These cells were not significantly different from wild-type cells under control conditions (wild-type, $AP_{90} = 12.3 \pm 1.0$ ($n = 8$); *AnkB*$^{+/-}$, $AP_{90} = 15.0 \pm 1.4$ ($n = 17$), where AP_{90} = time (in ms) for 90% repolarization of action potentials). However, after acute application of isoproterenol (1 μM) to simulate conditions of stress, action potentials in *AnkB*$^{+/-}$ cardiomyocytes developed spontaneous extrasystoles at both 1 and 5 Hz, whereas control cells did not. Both delayed after-depolarizations (DADs) and early after-depolarizations (EADs) were observed in *AnkB*$^{+/-}$ cells, and the DADs and EADs led to extrasystoles. The appearance of EADs, DADs and extrasystoles suggest that these arrhythmic mechanisms underlie the lethal arrhythmias seen in humans with the E1425G mutation, and might be caused by elevated $[Ca^{2+}]_i$[11]. A causative role of increased $[Ca^{2+}]_i$ in cardiac arrhythmia and congenital sudden cardiac death is an emerging area of interest, with current examples including gain-of-function mutations in the Ryr2 Ca^{2+}-release channel[12].

Elevation in the $[Ca^{2+}]_i$ transient in *AnkB*$^{+/-}$ cardiomyocytes can be rationalized by loss of Na/K ATPase isoforms[13,14]. A small reduction of Na/K ATPase would be expected to mimic effects of cardiac glycosides such as digitalis, a Na/K ATPase inhibitor[11]. Na/K ATPase inhibition results in increased $[Ca^{2+}]_i$ by first producing an increase in $[Na^+]_i$, leading to a reduction of Ca^{2+} extrusion by Ncx[13,14] into the extracellular space. In the face of unchanged Ca^{2+} entry by I_{Ca}, and combined with a small reduction in Ncx, the reduction of Na/K ATPase in *AnkB*$^{+/-}$ cells should lead to an increase in total cellular Ca^{2+}, as suggested by our data. Long-term reduction or increase in Ncx in animal models does not seem to produce a severe phenotype because of diverse compensatory mechanisms[15]. Therefore the loss of Na/K ATPase is probably the major contributor to elevated $[Ca^{2+}]_i$ transients in *AnkB*$^{+/-}$ ventricular myocytes. This study shows that ankyrin-B has an important involvement in regulating the coordinated expression of Ncx, the Na/K ATPase, $InsP_3R$, and possibly other ankyrin-binding proteins. Moreover, the ankyrin-B dysfunction in humans leads to lethal cardiac arrhythmias and type 4 long-QT syndrome. □

Methods

Human mutation analysis

Genomic DNA was prepared from peripheral blood lymphocytes. Mutation analysis was conducted by direct sequencing of the ankyrin-B gene. All 45 exons of the ankyrin-B gene were amplified using intronic primers (Supplementary Fig. 5).

Mouse ECG recordings

We performed and analysed mouse ECG recordings as described in the Supplementary Information.

AnkB$^{+/-}$ cardiomyocytes

GFP–ankyrin-B E1425G was created using standard molecular techniques. Neonatal cardiomyocytes were prepared, transfected[5] and imaged using Fluo3-AM[4]. Transfection was optimized for low GFP–ankyrin-B expression (levels undetectable without GFP-labelled antisera[5]). After Ca^{2+} imaging, cells were immunostained using indicated antisera and visualized using Alexa 568 so that signal would not interfere with Fluo3 fluorescence. For contraction experiments, over 100 cells were monitored for each condition. For rescue experiments, Ca^{2+} was monitored in over ten cells for each condition.

Immunoblotting and immunoprecipitations

We performed quantitative immunoblots using equal protein concentrations as described[4]. Adult heart immunoprecipitations were performed using standard techniques (lysis buffer: 1.5% Triton X-100, 0.5% deoxycholate plus × 2 protease inhibitor cocktail, most proteins were soluble except for $InsP_3R$ (40%)). Immunoblotting was performed using ^{125}I-labelled protein A, and intensities were quantified by phosphorimaging[5].

Immunostaining and imaging

Wild-type and *AnkB*$^{+/-}$ cells were prepared and imaged identically as described[5]. Antibodies used were: α-actinin, dystrophin and Dhpr (Sigma), $InsP_3R$ types 1 and 2 (ABR), pan $InsP_3R$ (Calbiochem), Pmca2, Ryr2 and Serca2 (ABR), GFP (Chemicon or Clontech), Ncx1 (RDI), Na/K ATPase α1 (Developmental Studies Hybridoma Bank; Upstate Biotechnology; M. Caplan) α2 (Upstate Biotechnology), Erg1 and connexin 43 (Chemicon), NaV1.6, Kir2.1, Kir2.3 and MinK (Alomone), $Na_V1.5$ (W. Catterall), Kcnq1 (K_VLqt1; Santa Cruz), and ankyrin-B monoclonal and affinity purified polyclonal immunoglobulin. Similar results were obtained in both isolated cardiomyocytes and in sections of adult cardiac muscle.

Patch-clamp methods

AnkB$^{+/-}$ and wild-type animals (1–3 months of age) were killed by an intraperitoneal injection of pentobarbital sodium (100 mg per kg). Single cardiomyocytes were isolated[16]. An Axopatch-200A or -200B amplifier (Axon Instruments) was used to measure membrane currents[16,17]. The patch pipette (1–3 MΩ) solution was (in mM): CsCl (130), NaCl (10), MgATP (5), HEPES (10), $MgCl_2$ (1), TEA-Cl (20) pH 7.2 (with CsOH). Superfusion solution 1 contained (in mM): NaCl (140), KCl (5), $MgCl_2$ (0.5), $CaCl_2$ (1.8), NaH_2PO_4 (0.33), glucose (5.5) and HEPES (5), pH 7.4, at 35–37 °C. Superfusion solution 2 was the same as solution 1 but with CsCl substituted for KCl +10 μm TTX. After conversion to whole-cell voltage clamp in solution 1, solution 2 was used to measure I_{Ca}. Test depolarizations followed 4 50-ms depolarizations to 0 mV at 1 Hz. A 500-ms ramp-depolarization from −90 mV to −40 mV was followed by a 50-ms period at −40 mV before test depolarizations.

Action potential recordings

Cardiomyocytes were superfused with solution 1. β-adrenergic stimulation of cells was produced by the addition of 1 μM isoproterenol to solution 1. Pipette filling solution was as above, except that KCl was substituted for CsCl (pH 7.2 with KOH). Axopatch 200A was used in current clamp mode to record action potentials. Current injections triggered action potentials at a constant rate (1 Hz, 5 Hz). We performed all experiments at 37 °C.

Confocal $[Ca^{2+}]_i$ imaging

Biorad MRC600 and Zeiss LSM510 microscopes were used with simultaneous electrical measurements to determine $[Ca^{2+}]_i$ (refs 16, 18). In parallel experiments, measurements of resting $[Ca^{2+}]_i$ were obtained by adding indo-1 (25 μM)[19] to the pipette filling solution, on a system made by the authors. Resting $[Ca^{2+}]_i$ was calculated as described[19].

Statistics

Data were analysed using either paired two-tailed *t*-tests or two-way analysis of variance, and *P* values <0.05 were considered significant. Data are expressed as means ± s.e.m.

Received 31 July; accepted 5 November 2002; doi:10.1038/nature01335.

1. Keating, M. T. & Sanguinetti, M. C. Molecular and cellular mechanisms of cardiac arrhythmias. *Cell* **104,** 569–580 (2001).
2. Mohler, P. J., Gramolini, A. O. & Bennett, V. Ankyrins. *J. Cell Sci.* **115,** 1565–1566 (2002).
3. Schott, J. J. *et al.* Mapping of a gene for long QT syndrome to chromosome 4q25-27. *Am. J. Hum. Genet.* **57,** 1114–1122 (1995).
4. Tuvia, S., Buhusi, M., Davis, L., Reedy, M. & Bennett, V. Ankyrin-B is required for intracellular sorting of structurally diverse Ca^{2+} homeostasis proteins. *J. Cell Biol.* **147,** 995–1008 (1999).
5. Mohler, P. J., Gramolini, A. O. & Bennett, V. The Ankyrin-B C-terminal domain determines activity of Ankyrin-B/G chimeras in rescue of abnormal inositol 1,4,5-trisphosphate and ryanodine receptor distribution in ankyrin-B (-/-) neonatal cardiomyocytes. *J. Biol. Chem.* **277,** 10599–10607 (2002).
6. Towbin, J. A. & Vatta, M. Molecular biology and the prolonged QT syndromes. *Am. J. Med.* **110,** 385–398 (2001).
7. Casimiro, M. C. *et al.* Targeted disruption of the Kcnq1 gene produces a mouse model of Jervell and Lange-Nielsen Syndrome. *Proc. Natl Acad. Sci. USA* **98,** 2526–2531 (2001).
8. Jenkins, S. M. & Bennett, V. Ankyrin-G coordinates assembly of the spectrin-based membrane skeleton, voltage-gated sodium channels, and L1 CAMs at Purkinje neuron initial segments. *J. Cell Biol.* **155,** 739–746 (2001).
9. Bennett, V. & Baines, A. J. Spectrin and ankyrin-based pathways: metazoan inventions for integrating cells into tissues. *Physiol. Rev.* **81,** 1353–1392 (2001).
10. Frank, J. S. & Garfinkel, A. in *The Myocardium* (ed. Langer, G. A.) 1–32 (Academic, San Diego, California, 1997).
11. Bers, D. M. *Excitation-Contraction Coupling and Cardiac Contractile Force* (Kluwer, Dordrecht, 2001).
12. Marks, A. R., Priori, S., Memmi, M., Kontula, K. & Laitinen, P. J. Involvement of the cardiac ryanodine receptor/calcium release channel in catecholaminergic polymorphic ventricular tachycardia. *J. Cell Physiol.* **190,** 1–6 (2002).
13. Blaustein, M. P. & Lederer, W. J. Sodium/calcium exchange: its physiological implications. *Physiol. Rev.* **79,** 763–854 (1999).
14. Reuter, H. *et al.* The Na^+-Ca^{2+} exchanger is essential for the action of cardiac glycosides. *Circ. Res.* **90,** 305–308 (2002).
15. Philipson, K. D. & Nicoll, D. A. Sodium-calcium exchange: a molecular perspective. *Annu. Rev. Physiol.* **62,** 111–133 (2000).
16. Santana, L. F., Kranias, E. G. & Lederer, W. J. Calcium sparks and excitation-contraction coupling in phospholamban-deficient mouse ventricular myocytes. *J. Physiol.* **503,** 21–29 (1997).
17. Santana, L. F., Gomez, A. M. & Lederer, W. J. Ca^{2+} flux through promiscuous cardiac Na^+ channels: slip-mode conductance. *Science* **279,** 1027–1033 (1998).
18. Gomez, A. M. *et al.* Defective excitation-contraction coupling in experimental cardiac hypertrophy and heart failure. *Science* **276,** 800–806 (1997).
19. duBell, W. H., Lederer, W. J. & Rogers, T. B. Dynamic modulation of excitation-contraction coupling by protein phosphatases in rat ventricular myocytes. *J. Physiol.* **493,** 793–800 (1996).

Supplementary Information accompanies the paper on *Nature*'s website (http://www.nature.com/nature).

© 2003 Nature Publishing Group

Acknowledgements We thank the type 4 long-QT family for participation. Research support was provided by the Howard Hughes Medical Institute, NIH, the Muscular Dystrophy Association, Canadian Institutes of Health, the Institut National de la Santé et de la Recherche Médicale (INSERM), and the programme Hospitalier de Recherche Clinique. We also thank C. Kontos and B. Knollman for discussions.

Competing interests statement The authors declare that they have no competing financial interests.

Correspondence and requests for materials should be addressed to V.B. (e-mail: benne012@mc.duke.edu).

NF-κB blockade and oncogenic Ras trigger invasive human epidermal neoplasia

Maya Dajee*, Mirella Lazarov*, Jennifer Y. Zhang, Ti Cai, Cheryl L. Green, Alan J. Russell, M. Peter Marinkovich, Shiying Tao, Qun Lin, Yoshiaki Kubo & Paul A. Khavari

Veterans Affairs Palo Alto Healthcare System and the Program in Epithelial Biology, Stanford University School of Medicine, Stanford, California 94305, USA
** These authors contributed equally to this work*

The nuclear factor NF-κB and oncogenic Ras can alter proliferation in epidermis, the most common site of human cancer[1,2]. These proteins are implicated in epidermal squamous cell carcinoma in mice[3–5], however, the potential effects of altering their function are uncertain. Whereas inhibition of NF-κB enhances apoptosis in certain tumours[6], blockade of NF-κB predisposes murine skin to squamous cell carcinoma[5,7]. Because therapeutics inhibiting Ras and NF-κB pathways are being developed to treat human cancer[8,9], it is essential to assess the effects of altering these regulators. The medical relevance of murine studies is limited, however, by differences between mouse and human skin, and by the greater ease of transforming murine cells. Here we show that in normal human epidermal cells both NF-κB and oncogenic Ras trigger cell-cycle arrest. Growth arrest triggered by oncogenic Ras can be bypassed by IκBα-mediated blockade of NF-κB, generating malignant human epidermal tissue resembling squamous cell carcinoma. Human cell tumorigenesis is dependent on laminin 5 and α6β4 integrin. Thus, IκBα circumvents restraints on growth promotion induced by oncogenic Ras and can act with Ras to induce invasive human tissue neoplasia.

To study Ras and NF-κB in a setting more relevant to human tumorigenesis, we expressed the active Ha-Ras Gly12Val mutant, NF-κB p65 and a stable NF-κB repressor mutant of IκBα[10] in human skin tissue. Primary human keratinocytes were retrovirally transduced and used to regenerate human skin on immune-deficient mice[11]. Tissue expressing IκBα alone showed mild hyperplasia, whereas expression of oncogenic Ras induced growth arrest with graft failure (Fig. 1a and Supplementary Table I). Although implicated in promoting features of neoplasia in other settings[12], the coexpression of oncogenic Ras with NF-κB subunits failed to support proliferation (Supplementary Fig. 1a). Notably, the coexpression of Ras and IκBα (Ras–IκBα) produced large neoplasms resembling human squamous cell carcinomas (SCCs) in 3 weeks (Fig. 1a and Supplementary Fig. 1b).

Rapidly growing Ras–IκBα tumours showed hallmarks of SCC. Histologically, Ras–IκBα human epidermis showed massive neoplasia with deep invasion through fat and into underlying muscle and fascia (Fig. 1a). There are no diagnostic markers for human SCC[2]; however, Ras–IκBα epidermal tumours showed changes in protein expression that have been reported as characteristic for SCC, including increases in vascular endothelial growth factor (VEGF) and matrix metalloproteinase 3 (MMP3), and a decrease in E-cadherin (Fig. 1b). Ras–IκBα tumours also showed a more than tenfold increase in mitotic index (Fig. 1b). Thus, Ras–IκBα epidermal neoplasia strongly resembles spontaneous human SCC.

To determine the relevance of these findings to epidermal cancer, we studied primary human cutaneous SCCs. p65 was redistributed to the cytoplasm both in Ras–IκBα tumours and in SCCs obtained from patients (Fig. 1c). In addition, immunoblots from ten consecutive SCCs showed that a subset of SCCs expressed increased

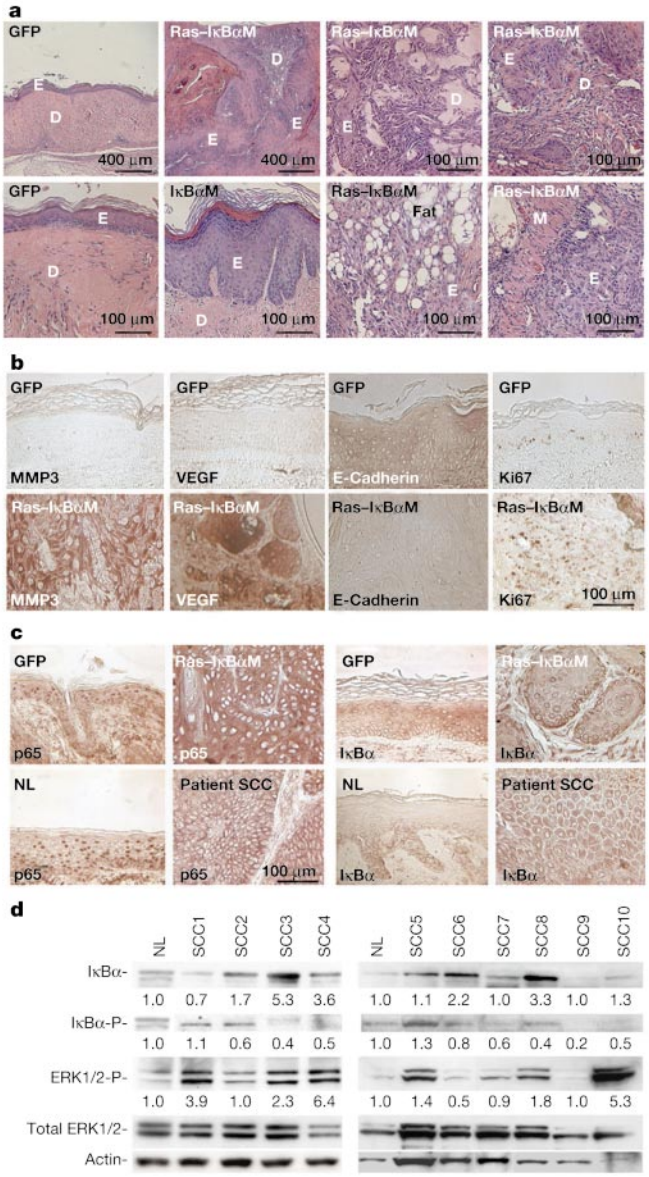

Figure 1 Ras and IκBα human epidermal neoplasia. **a**, Histology. Invasive epidermal neoplasia (E) through dermis (D), fat and muscle (M) **b**, Expression of MMP3, VEGF, E-cadherin and Ki67. **c**, Expression of p65 and IκBα in regenerated human epidermal tissue expressing either Ras–IκBα or GFP as compared with normal patient skin (NL) and spontaneously arising SCC. Note the loss of nuclear p65 distribution in both Ras–IκBα-induced and spontaneous epidermal tumours, and the widespread distribution of IκBα. **d**, Immunoblots of ten additional consecutive primary cutaneous SCCs.

© 2003 Nature Publishing Group